Available online at www.sciencedirect.com
SCIENCE DIRECT®
Journal of Sound and Vibration 292 (2006) 610–625
JOURNAL OF SOUND AND VIBRATION
www.elsevier.com/locate/jsvi

The effects of thickness on the impedance of a rectangular aperture in the presence of a grazing flow

K.S. Peat*, R. Sugimoto, J.L. Horner

Department of Aeronautical & Automotive Engineering, Loughborough University, Loughborough, LE11 3TU, UK

Received 26 February 2005; received in revised form 18 August 2005; accepted 18 August 2005
Available online 21 October 2005

Abstract

This paper presents an analytical investigation into the effect of a grazing mean flow upon the acoustic impedance of a rectangular aperture in a plate of finite thickness. Previous similar analytical works each made some simplifying approximation about the variation of the acoustic potential throughout the thickness of the aperture, such that they were valid only in either the thin or thick plate limits. In addition to providing a theoretical framework to correctly allow for a plate of any thickness, the results given here indicate the range of validity of the previous approximate theories.

Two different forms of matching conditions across the shear layer have been proposed in previous works. Equations and boundary element method (BEM) solutions for both variants are given here. Results from both forms are compared against some existing measured results. As the approximations regarding aperture thickness have now been removed, it is possible to be definitive as to which form of matching conditions gives the most accurate results for a given application. The analysis is shown to predict the reactance of the aperture very well, although the results for resistance show greater discrepancy against experimental values.

1. Introduction

It is common practice to use perforations in the walls of flow ducts as a sound-attenuating mechanism. Typical applications are in vehicle silencer systems, HVAC ducts and the nacelles of jet engines. The mean flow may be forced through the perforations, or be tangential to the plane of the perforations, or be a combination of both. It is well known that the mean flow has a marked effect upon the acoustic impedance of the orifices in the perforate, although the detailed mechanism and nature of that influence is still largely unknown. Attention is focused here on grazing flow past a rectangular aperture where the flow is turbulent, fully developed, and of low Mach number. Such conditions are typically found in exhaust silencers of internal combustion engines, although the perforations for this application are generally circular orifices or punched rectangular louvres.

The grazing flow effect on aperture impedance is generally accounted for by some empirical equation derived from one or more of the many experimental investigations [1–14] into the effect. There is much

*Corresponding author. Tel.: +44 1509 227232; fax: +44 1509 227275.
E-mail address: K.S.Peat@lboro.ac.uk (K.S. Peat).

0022-460X/$ - see front matter © 2005 Elsevier Ltd. All rights reserved.
doi:10.1016/j.jsv.2005.08.012

variation between experimental results, although general trends are observed through them all, such as an increase of orifice resistance and a decrease of orifice reactance with increasing mean flow. The variation can in part be explained by differences in the form of the mean flow, and in particular the boundary layer development, between the different sets of results. Theoretical models [5,15–19] of various complexity for the grazing flow effect on orifice impedance have at best predicted the general trends, but detailed validation against relevant experimental results has been poor. Furthermore, they have generally employed some form of empirical parameter.

Howe et al. [20] presented a purely theoretical analysis of the influence of grazing flow upon the impedance of a circular orifice when the flow is of low Mach number but high Reynolds number, such that viscous effects are unimportant except in the generation of vorticity. The orifice can then be assumed to be spanned by a vortex sheet of zero thickness. The analysis matches the flow fields above and below the plane of the orifice through continuity of pressure and displacement across the vortex sheet. The solution gives the distribution of the vertical component of the particle displacement across the aperture, which can then be integrated to yield the conductivity or impedance of the aperture. Howe, also gives a general method by which this form of an analysis can be extended to an aperture of finite thickness, both for rectangular [21] and circular [22] apertures. However, this method is approximate in so much as it is assumed that the vertical displacement does not vary throughout the thickness of the aperture. It is surmised [21,22] that this extension is therefore only valid for an orifice of small thickness to radius ratio, and also when the wavelength of disturbances on the vortex sheet is much greater than the orifice thickness.

In a further paper, Howe [23] has given an approximate method by which the same general form of analysis can be adapted for rectangular apertures of large thickness to width ratio. In this case, the fluid inside the cylindrical region of the aperture is assumed to be in uniform motion and is matched to the average pressure and displacement of the flow field above the shear layer, assuming the aperture to be of infinite thickness. Similar matching conditions are imposed in the lower plane of the aperture, although there is no shear layer to be considered here. To the author's knowledge, results from this thick aperture version of Howe's theory have never been compared to results either from experiments or the earlier theory for thinner apertures. Throughout this paper, results from the two forms of approximation for apertures of finite thickness are referred to as thin and thick aperture results, respectively.

In the application areas mentioned above and in the experimental measurements used for validation of the models in this paper [14,24], the flow tangential to the aperture will be highly turbulent such that the shear layer will be thick relative to the aperture size. Detailed theoretical and experimental studies [25–27] give evidence that across such a thick shear layer it is appropriate to apply continuity of normal particle velocity, rather than the condition of continuity of normal displacement which is correct across a vortex sheet of zero thickness. These observations prompted Jing et al. [28] to adapt the theory of Howe et al. [20,21] to impose continuity of pressure and normal velocity across the shear layer rather than continuity of pressure and displacement. This may be interpreted as an imprecise attempt to adapt the theory based on a vortex sheet to account for the fact that in reality the shear layer will have finite thickness. They assumed that the normal velocity was constant through the thickness of the aperture and hence one would expect their results to be valid only for apertures of small thickness to radius ratio, or for thin apertures. Jing et al. [28] introduced the shorthand particle displacement match (PDM) and particle velocity match (PVM) to distinguish the two cases, and the same terminology will be used here. They compared thin aperture analytical results for aperture impedance as a function of Mach number from both the PDM and PVM with measured values and concluded that the PVM values were more accurate for both resistance and reactance. Their experimental tests were conducted predominantly on apertures of large thickness to radius ratio.

Peat et al. [24] conducted a more exacting test by comparing results for orifice impedance as a function of Strouhal number from both the PDM and PVM with various sets of measured values. In respect of reactance, the conclusions of Jing et al. [28] were confirmed, since the PVM correctly predicted the trend if not the precise values of reactance as a function of Strouhal number. The results for resistance were rather more ambiguous, however. The orifices used in the experiments had dimensions typical of those found in vehicle silencer systems and had less thickness than those tested by Jing et al. [28], yet still they violated the thin wall approximation of the theory. Thus, concern remained that the differences between the theoretical and experimental results might

be attributable more to the thin aperture approximations than the matching conditions applied on the shear layer.

This paper extends the theory of Howe to consider the effects of aperture thickness precisely. The flow field within the thickness of the aperture is allowed to vary and it is matched to the external fields at both the top and bottom boundaries of the aperture. At the shear layer boundary, the PDM and PVM conditions are applied alternatively. Both sets of results are compared against results from the corresponding thin aperture theories, and the former results are also compared against results from the thick aperture theory. For simplicity, only rectangular apertures are considered such that the flow field within the thickness of the aperture can be considered as two-dimensional. This flow field is evaluated numerically by a boundary element method (BEM). The range of validity of the thin and thick aperture approximations then becomes clear. Finally, the BEM results are compared against some existing experimental results [24] for the impedance of circular orifices.

2. Governing equations

The early part of the analysis follows that of Howe et al. [20]. Consider an infinite rigid plate of thickness H in which there is a rectangular aperture of length $2s$ in the X-direction and width B in the Y-direction, as shown in Fig. 1. A uniform flow of velocity U in the X-direction is assumed to be present above the top surface of the plate, in $Z>0$. It is assumed that the fluid is incompressible and that the Reynolds number is large enough for viscosity to be neglected, except for its role in generating vorticity as the flow separates at the leading edge of the aperture. The aperture is spanned by a vortex sheet. It is assumed that the motion of this vortex sheet is two-dimensional and that there is no variation in the Y-direction across the width of the aperture. Within the thickness of the aperture, the flow field is then two-dimensional and is shown in cross-section in Fig. 2. The entire flow field is regarded as three distinct regions, coupled by flow boundaries Γ_U and Γ_L at the top and bottom surface of the aperture, respectively.

A uniform time-harmonic acoustic pressure fluctuation of frequency ω is applied across the aperture, with pressure magnitudes $p'_{1\infty}$ and $p'_{3\infty}$in the far-field of regions 1 and 3 respectively. Thus the velocity $\boldsymbol{q}_1$ in Region 1, $Z>0$, can be written as

$$\boldsymbol{q}_1 = U\mathbf{i} + \boldsymbol{q}'_1 \mathrm{e}^{-\mathrm{j}\omega t}, \tag{1}$$

where $\mathbf{i}$ is a unit vector in the X-direction and $\boldsymbol{q}'_1 \mathrm{e}^{-\mathrm{j}\omega t}$ is the particle velocity fluctuation. For fluctuations of small magnitude, the momentum equation can be linearized to give

$$\rho_0(-\mathrm{j}\omega + U\partial/\partial X)\boldsymbol{q}'_1 = -\nabla p'_1, \tag{2}$$

where $p'_r \mathrm{e}^{-\mathrm{j}\omega t}$ is the pressure fluctuation in region r. From the curl of Eq. (2) it is clear that a velocity potential exists such that

$$\boldsymbol{q}'_1 = \nabla(\Phi^+ + \Phi'_1) = \nabla\Phi'_1, \tag{3}$$

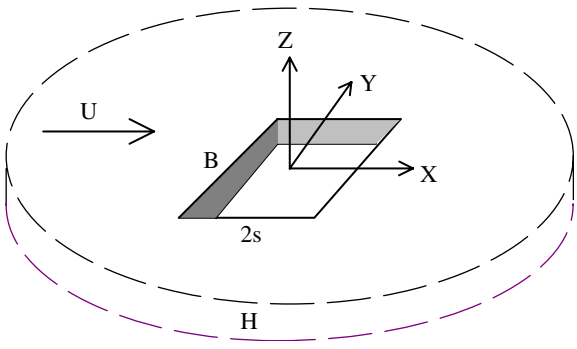

Fig. 1. One-sided flow past a rectangular aperture in an infinite plate.

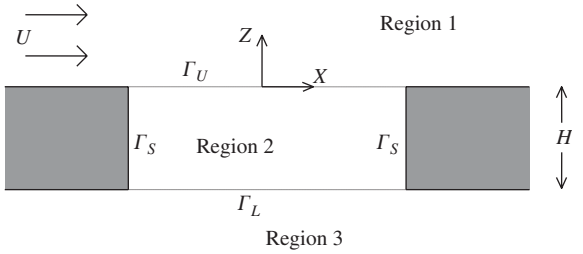

Fig. 2. Cross-section of the aperture of thickness h.

where Φ^+ is the constant far-field potential. Hence, from the incompressible continuity equation it follows that the velocity potential Φ_1' is subject to Laplace's equation. Substitution from Eq. (3) into Eq. (2) followed by integration gives

$$\rho_0(-\mathrm{j}\omega + U\partial/\partial X)\Phi_1' = -p_1' + p_{1\infty}', \tag{4}$$

where the constant of integration is the far-field applied pressure in Region 1. Now in Region 3, $Z<-H$, exactly the same relations apply with $U=0$, thus

$$-\mathrm{j}\omega\rho_0\Phi_3' = -p_3' + p_{3\infty}'. \tag{5}$$

Likewise in Region 2,

$$-\mathrm{j}\omega\rho_0\Phi_2' = -p_2' + c \tag{6}$$

for a general constant of integration c. Now there is no shear layer across the lower surface of the aperture, thus

$$\Phi_2' = \Phi_3' \text{ and } p_2' = p_2' \text{ on } \Gamma_L, \tag{7}$$

hence $c = p_{3\infty}'$.

2.1. Continuity of particle displacement across the vortex sheet

Howe et al. assumed that the pressure and particle displacement are continuous across the vortex sheet over the top surface of the aperture. From continuity of the pressure, it follows from Eqs. (4) and (6) that

$$\rho_0[(-\mathrm{j}\omega + U\partial/\partial X)\Phi_1' + \mathrm{j}\omega\Phi_2'] = p_{1\infty}' - p_{3\infty}' \text{ on } \Gamma_U. \tag{8}$$

Now the total derivative of acoustic displacement is the acoustic velocity, thus the Z-component alone gives

$$\left(-\mathrm{j}\omega + U\frac{\partial}{\partial X}\right)\frac{\partial\Phi_2'}{\partial Z} = -\mathrm{j}\omega\frac{\partial\Phi_1'}{\partial Z} \text{ on } \Gamma_U \tag{9}$$

for continuity of particle displacement across the shear layer. Non-dimensional variables are introduced where

$$\Phi_1' = \frac{\mathrm{j}\pi}{\rho_0\omega}(p_{1\infty}' - p_{3\infty}')\phi_1, \quad B = sb, \quad H = sh, \quad X = sx, \tag{10}$$

etc. such that Eqs. (8) and (9) can be re-written as

$$\left(1 + \frac{\mathrm{j}}{S}\frac{\partial}{\partial x}\right)\phi_1 - \phi_2 = \frac{1}{\pi} \text{ on } \Gamma_U \tag{11}$$

and

$$\left(1 + \frac{\mathrm{j}}{S}\frac{\partial}{\partial x}\right)\frac{\partial\phi_2}{\partial z} = \frac{\partial\phi_1}{\partial z} \text{ on } \Gamma_U, \tag{12}$$

respectively, where $S = \omega s/U$ is the Strouhal number.

Since the plate is assumed to be rigid, the velocity component normal to the plate is zero on $z=0$ and $z=-h$ except in the region of the aperture. Thus, from application of Green's Theorem in Regions 1 and 3,

$$\phi_{1i} = -\frac{1}{2\pi}\iint_{\Gamma_U}\frac{(\partial\phi_1/\partial z)}{r}\mathrm{d}\xi\mathrm{d}\eta \quad \text{and} \quad \phi_{3i} = \frac{1}{2\pi}\iint_{\Gamma_L}\frac{(\partial\phi_3/\partial z)}{r}\mathrm{d}\xi\mathrm{d}\eta \tag{13a,b}$$

on Γ_U and Γ_L, respectively, where $r=|\boldsymbol{r}(\xi,\eta)-\boldsymbol{r}_i(x,y)|$ and point i lies on Γ_U or Γ_L, respectively. Integration with respect to η and y leads to spanwise-averaged equations of the form [22]

$$\phi_1(x) = \frac{-1}{2\pi}\int_{-1}^{+1}\frac{\partial\phi_1(\xi)}{\partial z}R(x,\xi)\mathrm{d}\xi \quad \text{and} \quad \phi_3(x) = \frac{1}{2\pi}\int_{-1}^{+1}\frac{\partial\phi_3(\xi)}{\partial z}R(x,\xi)\mathrm{d}\xi, \tag{14a,b}$$

where

$$R(x,\xi) = \frac{1}{b}\int\int_{-b/2}^{+b/2}\frac{\mathrm{d}\eta\,\mathrm{d}y}{r} = -2\{\ln|x-\xi| + \mathbf{L}(x,\xi)\} \tag{15}$$

and

$$\mathbf{L}(x,\xi) = -\ln\left\{b+\sqrt{b^2+(x-\xi)^2}\right\} + \sqrt{1+(1/b)^2(x-\xi)^2} - (1/b)|x-\xi|. \tag{16}$$

Given the conditions on the lower boundary, Eq. (7), it follows from Eq. (14b) that

$$\phi_2(x) = \frac{1}{2\pi}\int_{-1}^{+1}\frac{\partial\phi_2(\xi)}{\partial z}R(x,\xi)\mathrm{d}\xi \ \text{ on } \ \Gamma_L. \tag{17}$$

Substitution from Eq. (14a) into Eq. (11), followed by use of Eq. (12), gives

$$\left(1+\frac{\mathrm{j}}{S}\frac{\partial}{\partial x}\right)^2\left[\frac{1}{2}\int_{-1}^{+1}\frac{\partial\phi_2(\xi)}{\partial z}R(x,\xi)\mathrm{d}\xi\right] + \pi\phi_2(x) = -1 \ \text{ on } \ \Gamma_U. \tag{18}$$

As a check on consistency, it may be noted that it is possible to recover earlier solutions from the formulation above. Firstly, in the limit of a plate of infinitesimal thickness, $\Gamma_L=\Gamma_U$ and it follows from Eqs. (17) and (18) that

$$\left\{\left(1+\frac{\mathrm{j}}{S}\frac{\partial}{\partial x}\right)^2+1\right\}\left[\frac{1}{2}\int_{-1}^{+1}\frac{\partial\phi_2(\xi)}{\partial z}R(x,\xi)\mathrm{d}\xi\right] = -1 \ \text{ on } \ \Gamma_U, \tag{19}$$

which is the solution of Howe et al. [20]. Secondly, for a thin wall $h\ll 1$ and provided the wavelength of the disturbance on the vortex sheet is large compared to h, Howe assumed that the vertical displacement of fluid in the aperture is independent of z, say $\partial\phi_2/\partial z = f(x)$. It follows from integration with respect to z that

$$\phi_2|_{\Gamma_L} = \phi_2|_{\Gamma_U} - h\frac{\partial\phi_2}{\partial z}. \tag{20}$$

Thus from Eqs. (17), (18) and (20)

$$\left\{\left(1+\frac{\mathrm{j}}{S}\frac{\partial}{\partial x}\right)^2+1\right\}\left[\frac{1}{2}\int_{-1}^{+1}\frac{\partial\phi_2(\xi)}{\partial z}R(x,\xi)\mathrm{d}\xi\right] + h\frac{\partial\phi_2}{\partial z} = -1 \ \text{ on } \ \Gamma_U \tag{21}$$

and again the solution of Howe [22] is recovered.

Eq. (18) can be re-written as

$$\left(1+\frac{\mathrm{j}}{S}\frac{\partial}{\partial x}\right)^2\left\{\int_{-1}^{+1}\left[\frac{1}{2}\frac{\partial\phi_2(\xi)}{\partial z}R(x,\xi)+\pi\phi_2(\xi)G(x,\xi)\right]\mathrm{d}\xi\right\} = -1 \ \text{ on } \ \Gamma_U, \tag{22}$$

where

$$G(x,\xi) = -S^2(x-\xi)H(x-\xi)\mathrm{e}^{\mathrm{j}S(x-\xi)}, \tag{23}$$

since the Green's function $G(x,\xi)$ then satisfies

$$\left(1+\frac{\mathrm{j}}{S}\frac{\partial}{\partial x}\right)^2 G(x,\xi)=\delta(x-\xi). \tag{24}$$

Eq. (22) can now be integrated with respect to the second-order differential operator to give

$$\int_{-1}^{+1}\left[\frac{1}{2}\frac{\partial\phi_2(\xi)}{\partial z}R(x,\xi)+\pi\phi_2(\xi)G(x,\xi)\right]\mathrm{d}\xi+(\lambda_1+\lambda_2 x)\mathrm{e}^{\mathrm{j}Sx}=-1 \text{ on } \Gamma_U \tag{25}$$

for arbitrary coefficients λ_1 and λ_2.

In Region 2, the solution is completely two-dimensional and hence, for rigid side walls Γ_S to the aperture, Green's Theorem gives

$$c_i\phi_{2i}=\frac{1}{2\pi}\int_{\Gamma_U}\left(\frac{\phi_2}{r}\frac{\partial r}{\partial n}-\ln(r)\frac{\partial\phi_2}{\partial z}\right)\mathrm{d}\xi+\frac{1}{2\pi}\int_{\Gamma_L}\left(\frac{\phi_2}{r}\frac{\partial r}{\partial n}+\ln(r)\frac{\partial\phi_2}{\partial z}\right)\mathrm{d}\xi+\frac{1}{2\pi}\int_{\Gamma_S}\frac{\phi_2}{r}\frac{\partial r}{\partial n}\,\mathrm{d}\Gamma, \tag{26}$$

where now $r=|\boldsymbol{r}(\xi,\varsigma)-\boldsymbol{r}_i(x,z)|$, and n is the outward normal to the boundaries. The value of coefficient c_i depends upon the location of point i, but in this paper point i will always be taken on a smooth portion of boundary at which $c_i=0.5$. A solution is sought for Eq. (26) subject to conditions (17) and (25) on Γ_L and Γ_U, respectively.

2.2. Continuity of normal particle velocity across the vortex sheet

Jing et al. [28] proposed the application of continuity of the normal particle velocity across the vortex sheet rather than the continuity of the particle displacement. This is given by

$$\frac{\partial\Phi_2'}{\partial Z}=\frac{\partial\Phi_1'}{\partial Z} \text{ on } \Gamma_U \tag{27}$$

or in terms of non-dimensional variables given by Eq. (10)

$$\frac{\partial\phi_2}{\partial z}=\frac{\partial\phi_1}{\partial z} \text{ on } \Gamma_U \tag{28}$$

and results in Eq. (18) regarding the boundary condition on Γ_U being replaced by

$$\left(1+\frac{\mathrm{j}}{S}\frac{\partial}{\partial x}\right)\left[\frac{1}{2}\int_{-1}^{+1}\frac{\partial\phi_2(\xi)}{\partial z}R(x,\xi)\mathrm{d}\xi\right]+\pi\phi_2(x)=-1 \text{ on } \Gamma_U. \tag{29}$$

This can be re-written as

$$\left(1+\frac{\mathrm{j}}{S}\frac{\partial}{\partial x}\right)\left\{\int_{-1}^{+1}\left[\frac{1}{2}\frac{\partial\phi_2(\xi)}{\partial z}R(x,\xi)+\pi\phi_2(\xi)G'(x,\xi)\right]\mathrm{d}\xi\right\}=-1 \text{ on } \Gamma_U, \tag{30}$$

where the Green's function $G'(x,\xi)$ is given by

$$G'(x,\xi)=-\mathrm{j}S(x-\xi)H(x-\xi)\mathrm{e}^{\mathrm{j}S(x-\xi)}, \tag{31}$$

which satisfies

$$\left(1+\frac{\mathrm{j}}{S}\frac{\partial}{\partial x}\right)G'(x,\xi)=\delta(x-\xi). \tag{32}$$

Eq. (30) can now be integrated with respect to the first-order differential operator to give

$$\int_{-1}^{+1}\left[\frac{1}{2}\frac{\partial\phi_2(\xi)}{\partial z}R(x,\xi)+\pi\phi_2(\xi)G'(x,\xi)\right]\mathrm{d}\xi+\lambda\mathrm{e}^{\mathrm{j}Sx}=-1 \text{ on } \Gamma_U \tag{33}$$

for an arbitrary coefficient λ.

A solution is sought for the integral equation (26) subject to conditions (17) and (33) on Γ_L and Γ_U, respectively, when continuity of the normal velocity across the vortex sheet is applied.

3. Solution of the governing equations

In order to solve the complete problem for an aperture of finite thickness, it is necessary to find the boundary integral equation (26) concerning Region 2 subject to the boundary conditions on Γ_L and Γ_U. The boundary condition on Γ_L is given by Eq. (17), and the boundary condition on Γ_U is given by Eq. (25) or (33) according to continuity of the displacement or the normal velocity, respectively. A boundary element procedure is used, whereby the entire boundary $\Gamma_L+\Gamma_U+\Gamma_S$ of the aperture is discretized into a finite number of elements with associated nodes, at which the values of ϕ_2 and $\partial\phi_2/\partial n$ are to be determined. For simplicity, the suffix 2 will be dropped from further equations since they all now refer to Region 2 only.

The boundary integral equation (26) can be written in matrix format as

$$\begin{bmatrix} A_1 & A_2 & A_3 \\ A_4 & A_5 & A_6 \\ A_7 & A_8 & A_9 \end{bmatrix} \begin{Bmatrix} \boldsymbol{\phi}_{\Gamma_U} \\ \boldsymbol{\phi}_{\Gamma_L} \\ \boldsymbol{\phi}_{\Gamma_S} \end{Bmatrix} = \begin{bmatrix} B_1 & B_2 \\ B_3 & B_4 \\ B_5 & B_6 \end{bmatrix} \begin{Bmatrix} (\partial\boldsymbol{\phi}/\partial z)_{\Gamma_U} \\ (\partial\boldsymbol{\phi}/\partial z)_{\Gamma_L} \end{Bmatrix}, \tag{34}$$

where the coefficients of sub-matrices A_{1-9} and B_{1-6} are all known. Similarly, Eqs. (17), (25) and (33) can now be written as

$$\{\boldsymbol{\phi}_{\Gamma_L}\} = [C]\{(\partial\boldsymbol{\phi}/\partial z)_{\Gamma_L}\}, \tag{35}$$

$$[D]\{\boldsymbol{\phi}_{\Gamma_U}\} = [E](\partial\boldsymbol{\phi}/\partial z)_{\Gamma_{\tilde{U}}} - \{\mathbf{1}\} - \lambda_1\{e^{jSx}\} - \lambda_2\{xe^{jSx}\} \tag{36}$$

and

$$[F]\{\boldsymbol{\phi}_{\Gamma_U}\} = [E](\partial\boldsymbol{\phi}/\partial z)_{\Gamma_{\tilde{U}}} - \{\mathbf{1}\} - \lambda\{e^{jSx}\}, \tag{37}$$

respectively, where again the coefficients of matrices $[C]$ $[D]$ $[E]$ and $[F]$ are known. To be precise,

$$(A_l)_{ij} = \int_{e_j} \frac{1}{r}\frac{\partial r}{\partial n}\,\mathrm{d}\Gamma - \delta_{ij}\pi,$$

where $l = 1, 2, \ldots, 9$ and δ_{ij} is the Kronecker delta

$$(B_l)_{ij} = \alpha \int_{e_j} \ln(r)\mathrm{d}\Gamma,$$

where $l = 1, 2, \ldots, 6$ and, $\alpha = 1$ for $l = 1,3,5$ and $\alpha = -1$ for $l = 2,4,6$

$$C_{ij} = \frac{1}{2\pi}\int_{e_j} R(x,\xi)\,\mathrm{d}\Gamma, \quad D_{ij} = \int_{e_j} \pi G(x,\xi)\,\mathrm{d}\Gamma,$$
$$E_{ij} = -\frac{1}{2}\int_{e_j} R(x,\xi)\,\mathrm{d}\Gamma, \quad F_{ij} = \int_{e_j} \pi G'(x,\xi)\,\mathrm{d}\Gamma.$$

For the solution in the case where continuity of the displacement is applied, substitution from Eqs. (35) and (36) into Eq. (34) gives

$$\begin{bmatrix} A_1D^{-1}E - B_1 & A_2C - B_2 & A_3 \\ A_4D^{-1}E - B_3 & A_5C - B_4 & A_6 \\ A_7D^{-1}E - B_5 & A_8C - B_6 & A_9 \end{bmatrix} \begin{Bmatrix} (\partial\boldsymbol{\phi}/\partial z)_{\Gamma_U} \\ (\partial\boldsymbol{\phi}/\partial z)_{\Gamma_L} \\ \boldsymbol{\phi}_{\Gamma_S} \end{Bmatrix} = \begin{bmatrix} A_1D^{-1} \\ A_4D^{-1} \\ A_7D^{-1} \end{bmatrix} (\{\mathbf{1}\} + \lambda_1\{\mathbf{e}^{\mathbf{jSx}}\} + \lambda_2\{\mathbf{x}\mathbf{e}^{\mathbf{jSx}}\}). \tag{38}$$

On the other hand, for the solution in the case where continuity of the normal velocity is applied, substitution from Eqs. (35) and (37) into Eq. (34) gives

$$\begin{bmatrix} A_1F^{-1}E - B_1 & A_2C - B_2 & A_3 \\ A_4F^{-1}E - B_3 & A_5C - B_4 & A_6 \\ A_7F^{-1}E - B_5 & A_8C - B_6 & A_9 \end{bmatrix} \begin{Bmatrix} (\partial\boldsymbol{\phi}/\partial z)_{\Gamma_U} \\ (\partial\boldsymbol{\phi}/\partial z)_{\Gamma_L} \\ \boldsymbol{\phi}_{\Gamma_S} \end{Bmatrix} = \begin{bmatrix} A_1F^{-1} \\ A_4F^{-1} \\ A_7F^{-1} \end{bmatrix} (\{\mathbf{1}\} + \lambda\{\mathbf{e}^{\mathbf{jSx}}\}). \tag{39}$$

The Kutta condition implies that the vortex sheet leaves the surface of the plate tangentially and it is implemented by requiring that the vertical component of velocity is zero on the first few upstream nodes of Γ_U. In the case where continuity of the particle displacement is applied, the first two upstream velocity values are taken to be zero and Eq. (38) can be re-arranged to replace them in the vector of unknowns by the unknown coefficients λ_1 and λ_2, with consequent changes to the first two columns of the matrix on the left-hand side. Eq. (38) then becomes represents a square system of linear equations which can be solved and, in particular, the normal velocity on the shear layer follows. In the case where the continuity of the normal velocity is applied, only the first normal velocity is taken to be zero and Eq. (39) can be re-arranged to replace this value in the vector of unknowns by the unknown coefficient λ, with consequent changes to the first column of the matrix on the left-hand side.

Once the solution of the normal velocity $\partial\phi/\partial z$ on the boundary Γ_U is obtained, the Rayleigh conductivity and the acoustic impedance of the aperture can be calculated. Now the Rayleigh conductivity of an aperture is given by

$$K_R = \mathrm{j}\rho_0\omega Q/(p_{1\infty} - p_{3\infty}), \tag{40}$$

where Q is the volume velocity through the aperture. Hence from Eq. (10)

$$\frac{K_R}{2R_e} = \Gamma - \mathrm{j}\Delta = -\frac{\pi}{2}\sqrt{\frac{\pi B}{2s}}\int_{-1}^{+1}\left.\frac{\partial\phi}{\partial z}\right|_{\Gamma_U}\mathrm{d}x, \tag{41}$$

where the mean effective radius of the aperture $R_e = \sqrt{2sB/\pi}$. Alternatively, the specific acoustic impedance of the aperture is given by

$$\varsigma = \theta - \mathrm{j}\chi = (p_{3\infty} - p_{1\infty})/\rho_0 c_0 u = 2\mathrm{j}SM \Bigg/ \left(\pi\int_{-1}^{+1}\left.\frac{\partial\phi}{\partial z}\right|_{\Gamma_U}\mathrm{d}x\right), \tag{42}$$

where u is the average velocity through the aperture and M is the Mach number of the mean flow. It is seen that the impedance is predicted to vary linearly with the Mach number, hence subsequent results are all given for ς/M or $\theta/M, \chi/M$.

4. Results

Prior to investigation of the effects of thickness of an aperture, it is of interest to determine the effect of the assumption that the motion of the vortex sheet is two-dimensional and the associated spanwise averaging of the velocity potential. Fig. 3 gives a comparison of PDM results for aperture impedance obtained using this assumption, together with results from a complete analysis where the potential and the displacement were allowed to vary with y. The results are for a square aperture of zero thickness, i.e. with an aspect ratio

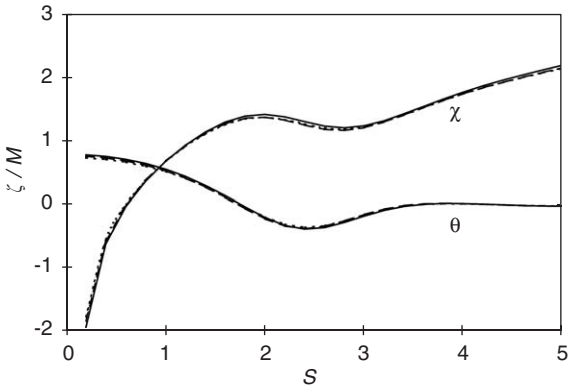

Fig. 3. Effect of spanwise averaging for an aperture of zero thickness (PDM analysis). —— analytical averaging; _____ numerical averaging; ----- with spanwise variation.

of $b/2 = 1$. A mesh of 40 elements in the streamwise direction and 20 elements across a half-span was used for both sets of analysis. Symmetry allows for meshing over only a half-span. The spanwise averaged results are obtained both by analytical integration and by numerical integration using the same number of spanwise strips as for the spanwise varying analysis. Fig. 3 shows that the effects of spanwise averaging are minimal even for an aperture of such small aspect ratio. There is a small but just distinguishable difference between the analytically and numerically integrated results, which indicates that in these results the mesh size has more bearing upon the error than whether or not one averages out the spanwise variation. There is no obvious reason why this conclusion should change for an aperture of non-zero thickness and the assumption is implicit in all of the results that follow.

All subsequent results also pertain to a square aperture. The reason for this choice is that, in the application area of vehicle exhaust systems at which this work is targeted, the perforations are generally circular orifices. As a first approximation, a circular orifice is modeled as a square aperture of equivalent area, for simplicity. Thus, the theoretical results are compared against experimental results for circular apertures. It may also be noted that a square aperture represents an exacting test case of the two-dimensional theory, which one would expect to model more accurately an aperture of high aspect ratio.

Results that demonstrate the effect of the thickness of the aperture upon its impedance are shown in Figs. 4–9. The results from the complete analysis as detailed in this paper are compared with results that use the various approximations, for both the PDM and PVM analysis. Analytical integration in the spanwise direction was used in all cases. The number of elements for integration across the aperture in the streamwise direction is kept the same for the thin, thick and BEM analyses. The number of elements required to ensure adequate convergence was checked at both the low and high limits of Strouhal number. For the BEM analysis,

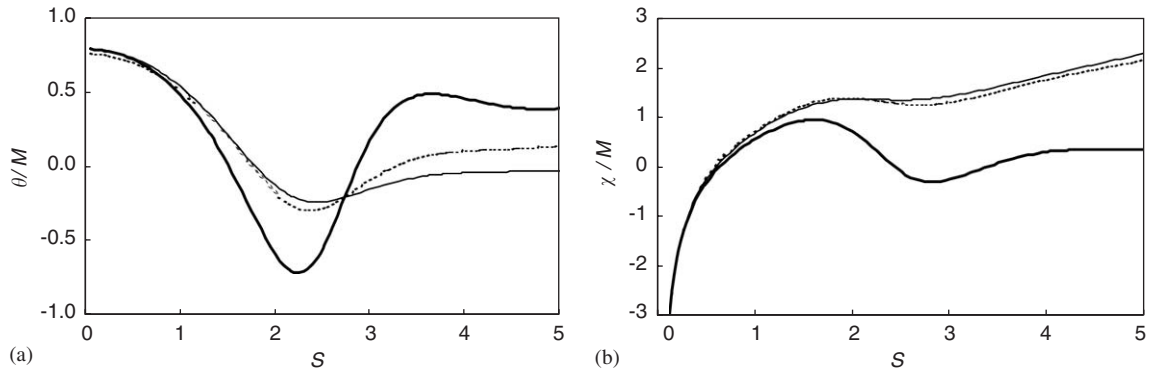

Fig. 4. Aperture impedance as a function of Strouhal number for a plate thickness $h = 0.1$ (PDM analysis): (a) resistance; (b) reactance. —— thin wall[20]; ——— thick wall[23]; ----- BEM.

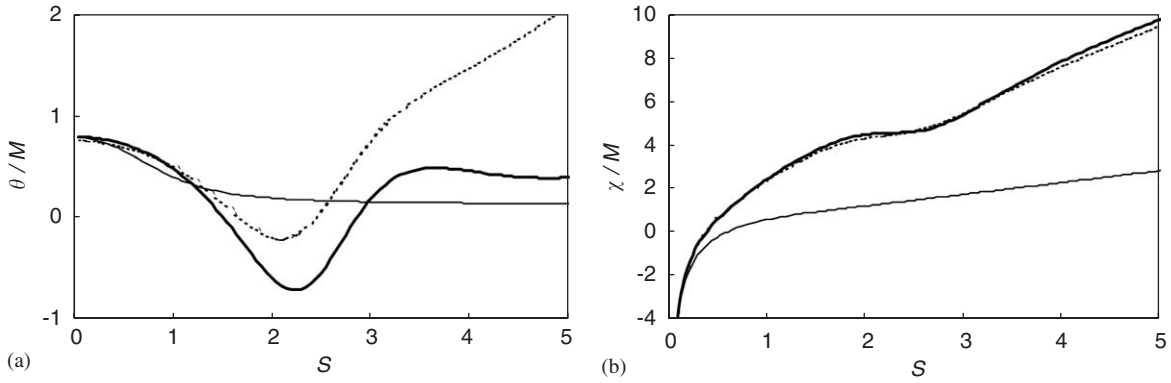

Fig. 5. Aperture impedance as a function of Strouhal number for a plate thickness $h = 2$ (PDM analysis): (a) resistance; (b) reactance. —— thin wall[20]; ——— thick wall[23]; ----- BEM.

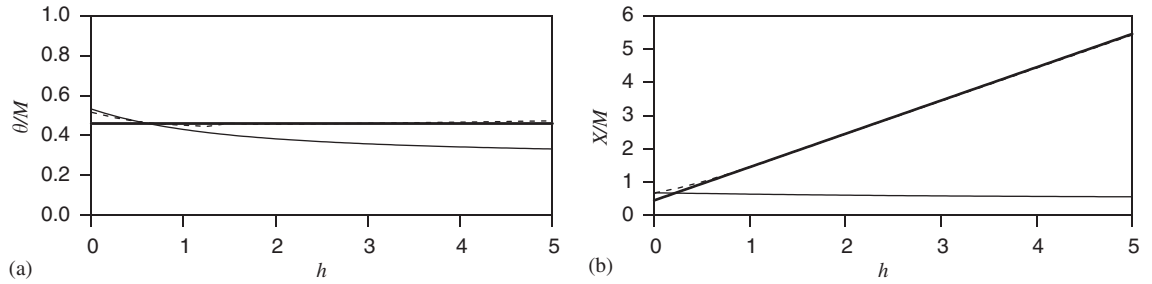

Fig. 6. Aperture impedance as a function of plate thickness for a Strouhal number $S = 1$ (PDM analysis): (a) resistance; (b) reactance. —— thin wall[20]; ——— thick wall[23]; ----- BEM.

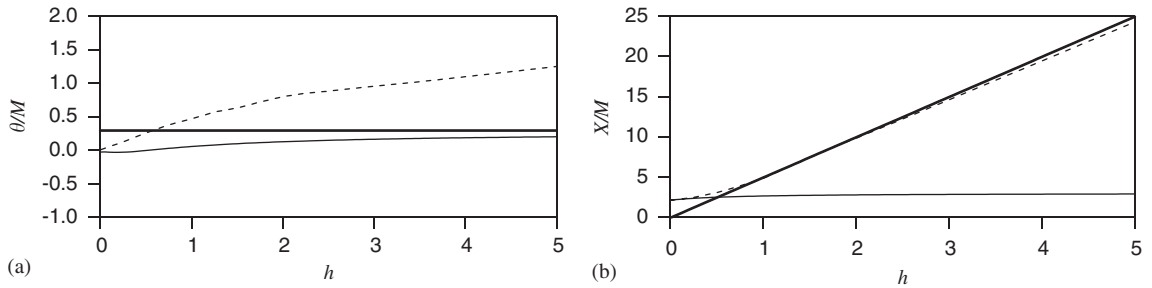

Fig. 7. Aperture impedance as a function of plate thickness for a Strouhal number $S = 5$ (PDM analysis): (a) resistance; (b) reactance. —— thin wall[20]; ——— thick wall[23]; ----- BEM.

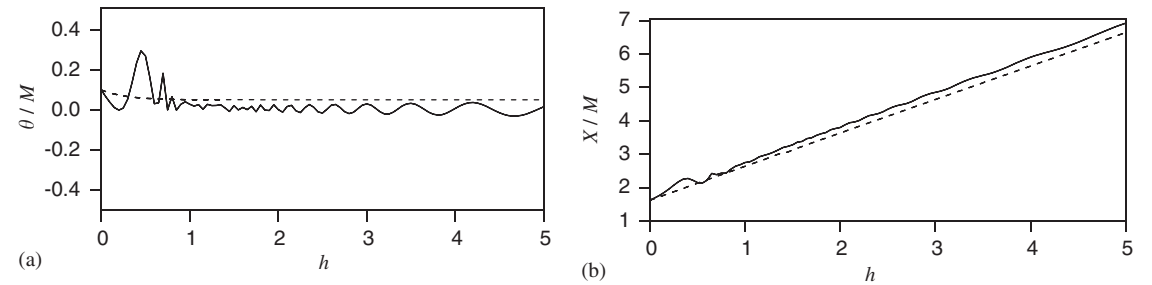

Fig. 8. Aperture impedance as a function of plate thickness for a Strouhal number $S = 1$ (PVM analysis): (a) resistance; (b) reactance. —— thin wall[28]; ----- BEM.

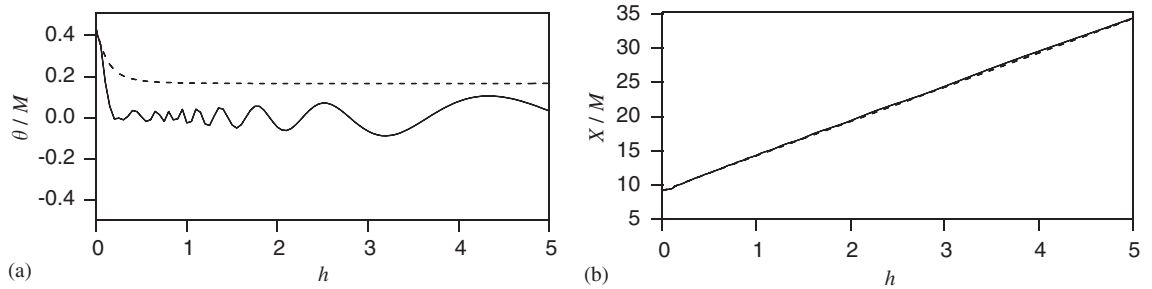

Fig. 9. Aperture impedance as a function of plate thickness for a Strouhal number $S = 5$ (PVM analysis): (a) resistance; (b) reactance. —— thin wall[28]; ----- BEM.

the element size on Γ_S has been kept as close as possible to that on Γ_U and Γ_L, subject to their being at least five elements. As a further check, it was found that the results of Howe et al. [20] for an aperture of infinitesimal thickness could be recovered from the BEM analysis for very small but non-zero h.

Figs. 4 and 5 show the aperture resistance and reactance for varying Strouhal number for plate thickness $h = 0.1$ and 2, respectively, using the PDM analysis. A comparison is given between the BEM results and results using both the thin and thick plate approximations. For the reactance in particular, the BEM results are seen to be close to the thin plate results in Fig. 4, where $h = 0.1$, and to the thick plate results in Fig. 5, where $h = 2$, as one might expect. Figs. 6 and 7 show the aperture resistance and reactance for varying plate thickness for a Strouhal number $S = 1$ and 5,respectively, using the PDM analysis. Again, a comparison is given between the BEM results and results using both the thin and thick plate approximations. It is seen from the results for reactance that the thin plate approximation is only valid for very small h, although the limit rises with Strouhal number up to about $h = 0.3$ when $S = 5$. The thick plate approximation appears valid for $h > 0.5$ at $S = 1$, rising to $h > 0.75$ at $S = 5$. In contrast, both the thin and thick plate approximations give poor values for the variation of resistance with plate thickness. Indeed the thick wall theory indicates that there is no variation in resistance at all with plate thickness. It should, however, be noted that the magnitude of the resistance is very small as compared to the reactance and thus absolute errors are far more noticeable in resistance values.

Results of the aperture impedance as a function of plate thickness from the PVM method are shown in Figs. 8 and 9 for Strouhal numbers of 1 and 5, respectively. At $S = 1$ the thin plate approximation is seen to give similar values to the BEM solution for all plate thicknesses, although the former results display an instability which is not seen in the latter. In contrast at $S = 5$ the thin plate approximation results for resistance are subject to substantial error except at very small plate thickness, but the reactance values remain accurate for all plate thicknesses. Again, absolute errors are far more noticeable in the resistance values, which have much smaller magnitude than the reactance values.

If Eqs. (38) and (39) are used for calculation of the BEM results for the PDM and PVM analysis, respectively, then an instability is noted in the vicinity of $h = 1.4$ in all of the results shown in Figs. 6–9. This instability can be removed by enforcement of the continuity equation for the overall problem. The final row in the partitioned matrix systems of both Eqs. (38) and (39) was replaced by

$$\begin{bmatrix} 1 & -1 & 0 \end{bmatrix} \begin{Bmatrix} (\partial \boldsymbol{\phi}/\partial z)_{\Gamma_U} \\ (\partial \boldsymbol{\phi}/\partial z)_{\Gamma_L} \\ \boldsymbol{\phi}_{\Gamma_S} \end{Bmatrix} = [0]$$

to enforce

$$\int_{\Gamma_U} (\partial \phi/\partial z)_{\Gamma_U} \mathrm{d}\xi = \int_{\Gamma_L} (\partial \phi/\partial z)_{\Gamma_L} \mathrm{d}\xi.$$

Although this treatment was effective in removal of the instability, a larger number of boundary elements was required along the shear layer as compared to the original formulation, before the results converged to a stable solution.

Figs. 10–13 show the distribution of normal velocity across the full span of the aperture on both its upper and lower surfaces, as given by the PVM method. Figs. 10–12 are for apertures of varying thickness, namely $h = 0.2$, 1 and 5, respectively, at a Strouhal number $S = 1$. It is seen that for $h = 0.2$ and 5, the distributions over the top and bottom surfaces of the aperture at $S = 1$ are nearly equal, as assumed by the thin wall theory, whereas at the intermediate thickness $h = 1$ the profiles are much more dissimilar. At higher Strouhal numbers, the velocity distribution on both surfaces has a distinct waveform of quite different amplitudes on the two surfaces, as seen in Fig. 13. This figure shows the relative distributions for $S = 5$ and $h = 0.2$, but the differences between the velocity distributions on the top and bottom surfaces remain equally marked for all apertures of greater thickness.

Finally, in Figs. 14–16, BEM results from both the PDM and PVM analyses are compared with experimental measurements of aperture impedance as given by Peat et al. [24], for three different sizes of aperture. The experiments were conducted on sections of perforated sheet containing an array of circular

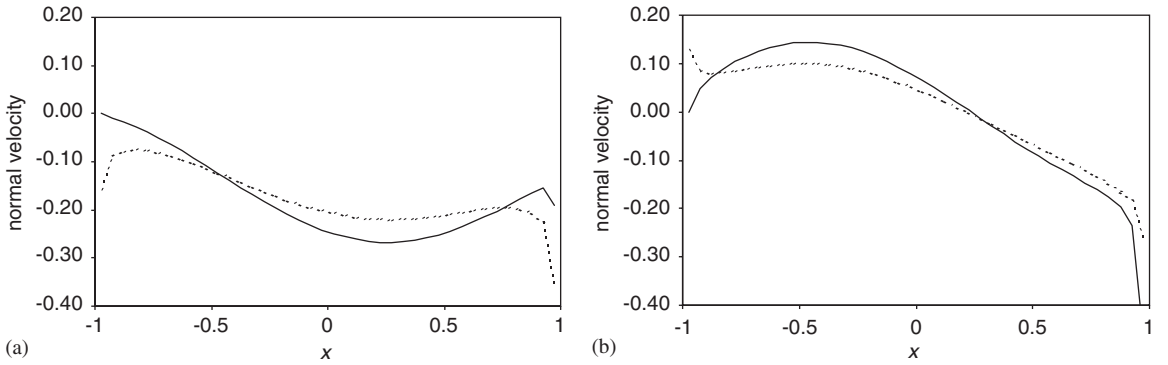

Fig. 10. Distribution of normal velocity over the upper and lower surfaces of an aperture of thickness $h = 0.2$, $S = 1$ (PVM analysis): (a) real part; (b) imaginary part. —— upper surface; - - - - - lower surface.

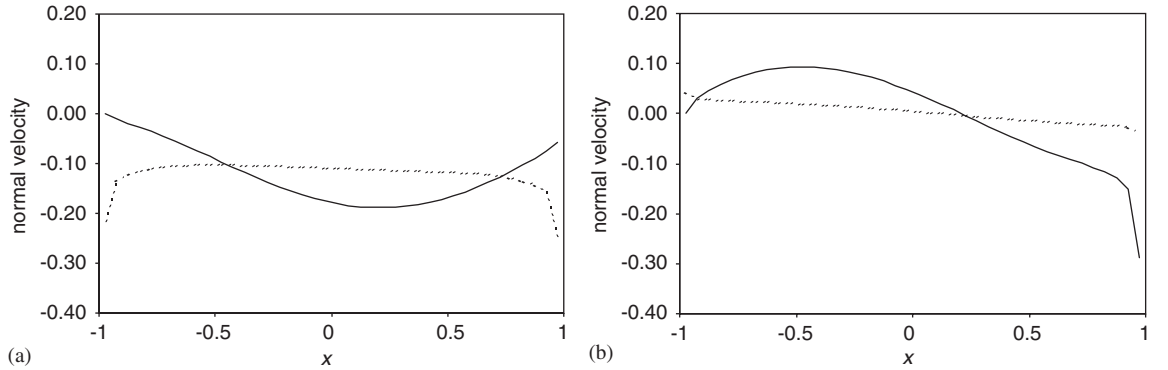

Fig. 11. Distribution of normal velocity over the upper and lower surfaces of an aperture of thickness $h = 1$, $S = 1$ (PVM analysis): (a) real part; (b) imaginary part. —— upper surface; - - - - - lower surface.

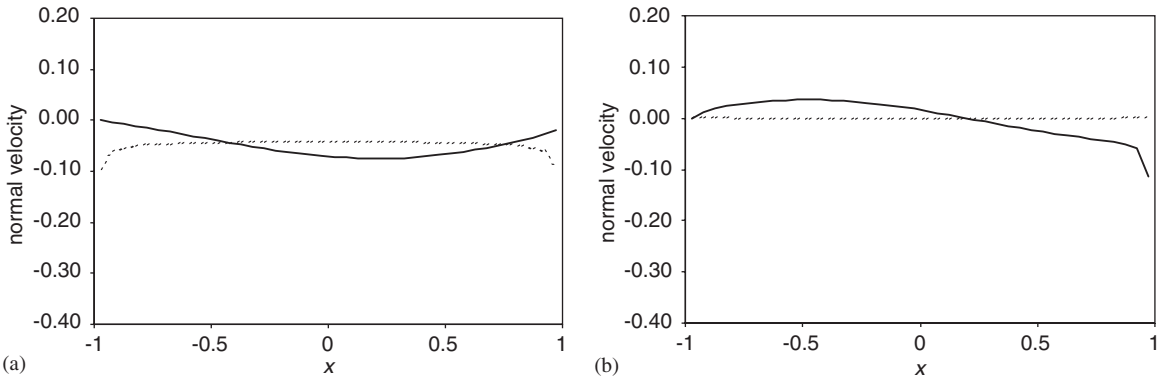

Fig. 12. Distribution of normal velocity over the upper and lower surfaces of an aperture of thickness $h = 5$, $S = 1$ (PVM analysis): (a) real part; (b) imaginary part. —— upper surface; - - - - - lower surface.

orifices. The Mach number of the mean flow was 0.085 in all of the tests. The results are presented in the form of impedance per single orifice, taking into account the interference effect between orifices as given by Rschevkin [29] for the zero mean flow case. Results for orifices of 4 mm diameter and thicknesses of 2, 3 and 5 mm are shown in Figs. 14–16, respectively. These values, particularly at the smallest thickness, are typical of orifice sizes used in the perforates of exhaust systems. The BEM analysis presented here is for the impedance

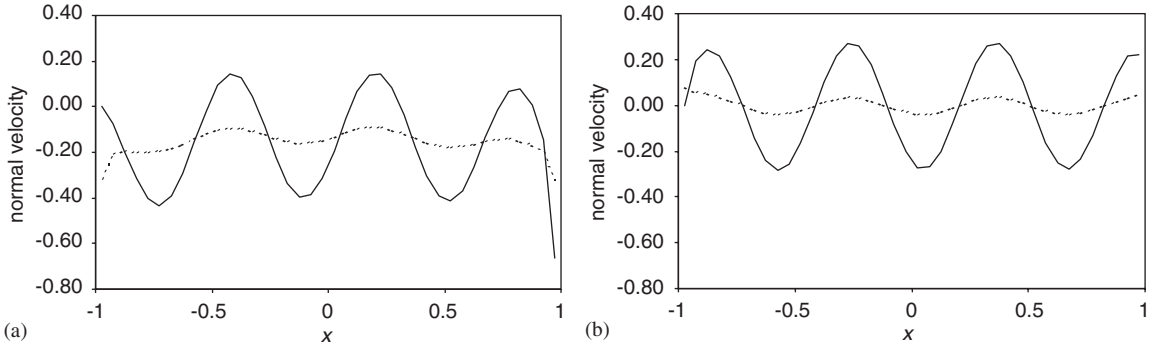

Fig. 13. Distribution of normal velocity over the upper and lower surfaces of an aperture of thickness $h = 0.2$, $S = 5$ (PVM analysis): (a) real part; (b) imaginary part. —— upper surface; ----- lower surface.

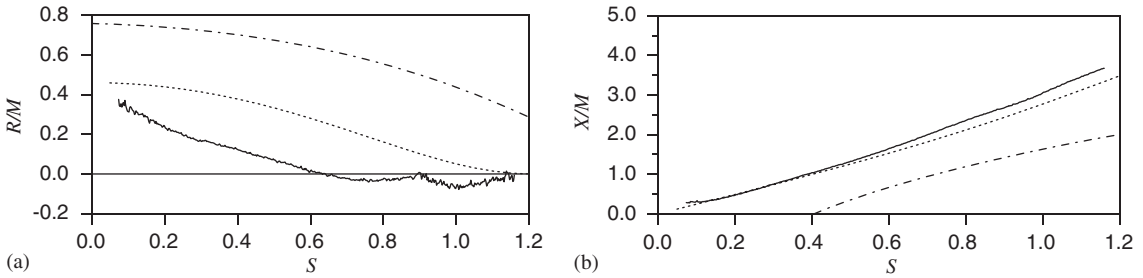

Fig. 14. Impedance of a circular orifice of diameter 4 mm, thickness 2 mm: (a) resistance; (b) reactance. ———— measured [24]; ———— PDM; ----- PVM.

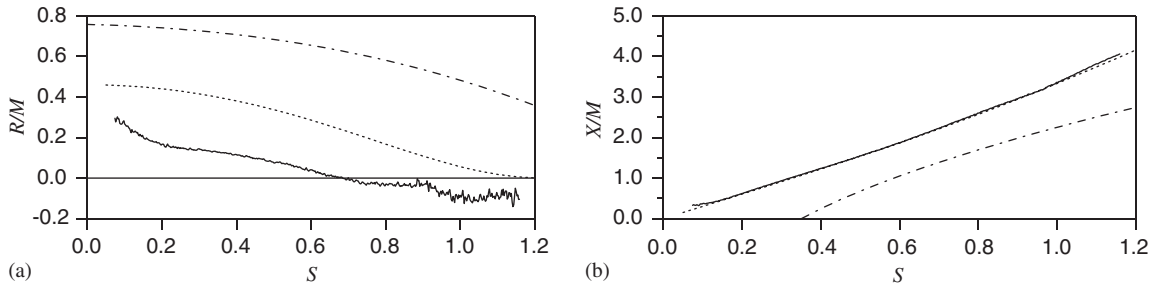

Fig. 15. Impedance of a circular orifice of diameter 4 mm, thickness 3 mm: (a) resistance; (b) reactance. ———— measured [24]; ———— PDM; ---- PVM.

of rectangular apertures. The results shown for comparison with experimental results are for square apertures of the same equivalent area as the circular orifices of the experiments, which results in values of $h = 1.13$, 1.7 and 2.82 for Figs. 14–16, respectively.

The results for reactance in Figs. 14–16 indicate that the PVM results are to be preferred to the PDM results. Indeed they model the experimental results to a very high degree of accuracy, especially in view of the fact that experimental results for a circular orifice have been compared against theoretical results for an equivalent square aperture. Unfortunately, the results for resistance are not as conclusive, although the PVM results are definitely better than the PDM results, which was not obviously the case when using the thin aperture approximations [24].

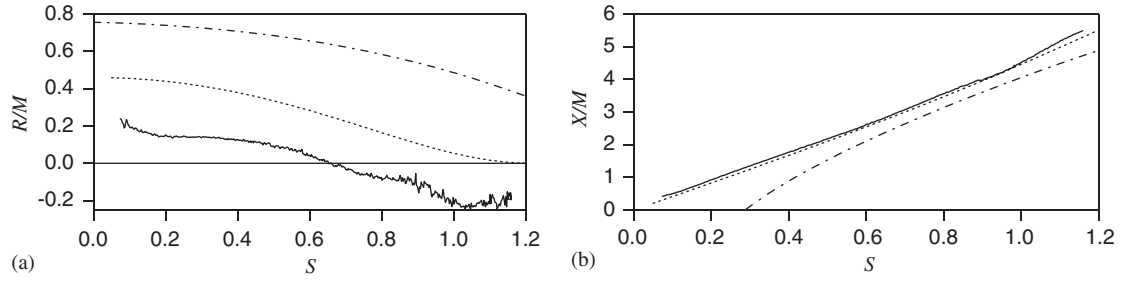

Fig. 16. Impedance of a circular orifice of diameter 4 mm, thickness 5 mm: (a) resistance; (b) reactance. measured [24]; ——————— PDM; ----- PVM.

It was noted in earlier work [24] which used the thin aperture approximation that the PDM results for resistance gave a better fit to experimental data when the mean flow velocity in the theory was taken to be the convection velocity of vorticity. This was a rational argument, since the only influence of mean flow in the theory is upon creation of the shear layer. The effect would be that all of the theoretical results in Figs. 14–16 would be compressed into a Strouhal number range of 0 to 0.6, rather than 0 to 1.2 as shown. However, the BEM results for reactance as given here, particularly for the PVM method, demonstrate very clearly that a Strouhal number based upon the mean flow velocity is the correct choice in the theory. The resistance results in Figs. 14–16 for both PDM and PVM would actually still benefit from the given redefinition of the theoretical Strouhal number, at least as regards prediction of the Strouhal number at which the resistance becomes negative. This is of particular interest because it marks the beginning of a Strouhal number in which the orifice generates self-noise and flow-generated noise, particularly whistles, are a problematic feature of perforates in exhaust systems. Thus the ability to predict the Strouhal number regime at which this problem occurs would be extremely valuable. Although a redefinition of the Strouhal number is now ruled out, it may be observed from Figs. 14 to 16 that the BEM results for resistance differ from the experimental results by virtually a constant shift alone. Given this shift, both the magnitude of resistance and the Strouhal number regime of negative resistance would be predicted accurately. Whether any rational explanation can be found to apply such a shift to either the experimental or theoretical results is quite another matter. It must also be remarked upon yet again that the magnitude of the resistance is very small such that any errors in the experimentation or shortcomings of the theoretical approach have a large relative effect upon the resistance as compared to the reactance.

The results given above have been computed for real frequencies ω. Howe [23] derived an approximate analytic continuation of the linear impedance function into the complex frequency plane to predict the frequency of the lowest self-sustained oscillation of the shear layer, for which the response amplitude increases exponentially with time. In practice, the amplitude will be limited by nonlinear mechanisms that are ignored by linear perturbation theory, but the frequency predicted by the latter was similar to that observed experimentally. It may be argued that at frequencies close to this tonal frequency, which essentially lies at the minimum point of negative resistance, the impedance ratio given by linear theory could be incorrect since the response amplitudes are limited by nonlinear mechanisms. The quality of the PVM results in Figs. 14–16 throughout the Strouhal number range would imply that this is not a problem and that the impedance ratio is governed primarily by physical attributes of the aperture, in particular the thickness, rather than by the mechanism which limits the response amplitudes.

5. Conclusions

An entirely analytical method, that fully accounts for thickness of the aperture, has been presented for the evaluation of the effect of grazing flow upon the impedance of rectangular apertures. Results from this analysis have been evaluated numerically by a BEM method and compared with results from earlier theories, each of which involved some form of approximation pertaining to the aperture thickness. These comparisons indicate the limits of accuracy and application of the various previous approximate theories.

For very thin shear layers, such that the PDM conditions are appropriate, it is shown that the thin plate approximation is only valid for infinitesimal aperture thickness, whereas the thick plate approximation gives a reasonable estimate of impedance when the thickness to length ratio of an aperture is greater than about 0.3, at high Strouhal numbers, the resistance value from the thick plate approximation is inaccurate for all thicknesses of aperture.

Previous work has indicated that the effects of a shear layer that is thick relative to the aperture size can be modeled effectively, if imprecisely, by applying PVM conditions to the underlying analysis for a thin shear layer. The work made use of a thin plate approximation. It has been shown in this paper that the thin plate approximation for PVM analysis gives quite accurate results of impedance for all aperture thicknesses, in comparison to results from the PVM analysis with full account taken of aperture thickness. However, once again the resistance becomes more inaccurate as the Strouhal number increases.

Theoretical values of aperture impedance for square apertures, from the current analysis with full account taken of aperture thickness, have been compared against existing experimental results for fully developed turbulent flow past circular orifices of equivalent area. The flow conditions, orifice shape and size are all typical of the situations encountered in vehicle exhaust silencers. The PVM matching conditions are shown to give impedance results that are much closer in comparison to the experimental results than results from the use of PDM matching conditions. This confirms earlier work that suggested the effect of a shear layer that is thick relative to the aperture size can be modeled effectively by use of PVM matching conditions. In particular, it is shown that in this way the reactance of an orifice in a fully developed turbulent grazing flow can be predicted very accurately.

Acknowledgments

The work presented in this paper was supported by the EC-project ARTEMIS (GRD-2000-25507). The authors would like to thank Prof J.-G. Ih and Mr. S.-Y. Lee of KAIST, Korea, for their help in the presentation of their experimental data.

References

[1] G.D. Garrison, Suppression of combustion oscillations with mechanical damping devices, *Pratt and Whitney Aircraft Rep. PWA FR3299* (1969).
[2] D. Ronneberger, The acoustic impedance of holes in the wall of flow ducts, *Journal of Sound and Vibration* 24 (1972) 133–150.
[3] P.D. Dean, An in situ method of wall acoustic impedance measurements in flow duct, *Journal of Sound and Vibration* 34 (1974) 97–130.
[4] A.B. Bauer, Impedance theory and measurements on porous acoustic liners, *Journal of Aircraft* 14 (1977) 720–728.
[5] A.S. Hersh, B. Walker, M. Bucka, Effect of the grazing flow on the acoustic impedance of Helmholtz resonators consisting of single and clustered orifices, *AIAA Paper 78-1124*, 1978.
[6] J.W. Sullivan, A method for modeling perforated tube muffler components. II. Application, *Journal of the Acoustical Society of America* 66 (1979) 779–788.
[7] K. Jayaraman, K. Yam, Decoupling approach to modeling perforated tube muffler components, *Journal of the Acoustical Society of America* 69 (1981) 390–396.
[8] A. Goldman, R.L. Panton, Measurement of the acoustic impedance of an orifice under a turbulent boundary layer, *Journal of the Acoustical Society of America* 60 (1976) 1397–1404.
[9] A. Goldman, C.H. Chung, Impedance of an orifice under a turbulent boundary layer with pressure gradient, *Journal of the Acoustical Society of America* 71 (1982) 573–579.
[10] K.N. Rao, M.L. Munjal, Experimental evaluation of impedance of perforate with grazing flow, *Journal of Sound and Vibration* 108 (1986) 283–295.
[11] J.W. Kooi, S.L. Sarin, An experimental study of the acoustic impedance of Helmholtz resonator arrays under a turbulent boundary layer, *AIAA Paper 81-1998* (1981).
[12] A. Cummings, The effects of grazing turbulent pipe-flow on the impedance of an orifice, *Acustica* 61 (1986) 233–242.
[13] R. Kirby, A. Cummings, The impedance of perforated plates subjected to grazing gas flow and backed by porous media, *Journal of Sound and Vibration* 217 (1998) 619–636.
[14] S.-H. Lee, J.-G. Ih, Empirical model of the acoustic impedance of a circular orifice in grazing mean flow, *Journal of the Acoustical Society of America* 114 (2003) 98–113.
[15] M.S. Howe, The influence of grazing flow on the acoustic impedance of a cylindrical wall cavity, *Journal of Sound and Vibration* 67 (1979) 533–544.

[16] A.E. Walker, A.F. Charwat, Correlation of the effects of grazing flow on the impedance of Helmholtz resonators, *Journal of the Acoustical Society of America* 72 (1982) 550–555.
[17] A. Ronneberger, The dynamics of shearing flow over a cavity—a visual study related to the acoustic impedance of small orifices, *Journal of Sound and Vibration* 71 (1980) 565–581.
[18] S. Kaji, M. Hiramoto, T. Okazaki, Acoustic characterization of holes exposed to grazing flow, *Bulletin of the Japanese Society of Mechanical Engineers* 27 (1984) 2388–2396.
[19] A.J. Rice, A theoretical study of the acoustic impedance of orifices in the presence of a steady grazing flow, *NASA TM X-71903* (1976).
[20] M.S. Howe, M.I. Scott, S.R. Sipcic, The influence of tangential mean flow on the Rayleigh conductivity of an aperture, *Proceedings of the Royal Society of London A* 452 (1996) 2302–2317.
[21] M.S. Howe, Influence of wall thickness on Rayleigh conductivity and flow-induced aperture tones, *Journal of Fluids and Structures* 11 (1997) 351–366.
[22] M.S. Howe, *Acoustics of Fluid–Structure Interactions*, Cambridge University Press, UK, 1998.
[23] M.S. Howe, Low Strouhal number instabilities of flow over apertures and wall cavities, *Journal of the Acoustical Society of America* 102 (1997) 772–780.
[24] K.S. Peat, J.-G. Ih, S.-H. Lee, The acoustic impedance of a circular orifice in grazing mean flow: comparison with theory, *Journal of the Acoustical Society of America* 114 (2003) 3076–3086.
[25] P.A. Nelson, N.A. Halliwell, P.E. Doak, Fluid dynamics of a flow excited resonance, part I: Experiment, *Journal of Sound and Vibration* 78 (1981) 15–38.
[26] P.A. Nelson, N.A. Halliwell, P.E. Doak, Fluid dynamics of a flow excited resonance, part II: Flow acoustic interaction, *Journal of Sound and Vibration* 91 (1983) 375–402.
[27] W.J. Worraker, N.A. Halliwell, Jet engine liner impedance: an experimental investigation of cavity neck flow/acoustics in the presence of a Mach 0.5 tangential shear flow, *Journal of Sound and Vibration* 103 (1985) 573–592.
[28] X. Jing, X. Sun, J. Wu, K. Meng, Effect of grazing flow on the acoustic impedance of an orifice, *AIAA Journal* 39 (2001) 1478–1484.
[29] S.N. Rschevkin, *A Course of Lectures on the Theory of Sound*, Pergamon Press, Oxford, 1963.